Response of the inner magnetosphere and the plasma sheet to a sudden impulse

K. Keika,[1] R. Nakamura,[1] W. Baumjohann,[1] A. Runov,[1,2] T. Takada,[1,3] M. Volwerk,[1,4] T. L. Zhang,[1] B. Klecker,[4] E. A. Lucek,[5] C. Carr,[5] H. Rème,[6] I. Dandouras,[6] M. André,[7] and H. Frey[8]

[1] The passage of an interplanetary shock caused a sudden compression of the magnetosphere between 0900 UT and 0915 UT on 24 August 2005. An estimate of the shock normal from solar wind data obtained by Geotail upstream of the bow shock indicates symmetric compression with respect to the noon-midnight meridian. Compression-related disturbances of the magnetic and electric field and plasma motion were observed by Double Star Program (DSP) Tan Ce 1 (TC1) and Tan Ce 2 (TC2) in the inner magnetosphere and by the Cluster spacecraft in the dawnside plasma sheet. DSP/TC1 and TC2 observations suggest that the disturbances in the inner magnetosphere are propagating from the dayside magnetopause. Cluster S/C 4 observations indicate that the front normal of the disturbances in the dawnside plasma sheet is $\phi \sim 180°$ at 0902:50 UT and $\phi = 107°$ at 0904:34 UT, where ϕ is the longitude in GSM coordinates, if we assume that the measured electric field is on the front plane and the normal lies on the $X–Y$ plane. The timing analysis applied to magnetic field data from the four Cluster spacecraft independently gives a front normal, which is calculated to be $\phi = 131°$ at about 0904:20 UT. Shock-associated magnetic and electric field disturbances propagating from both the dayside and flank magnetopauses are detected in the plasma sheet; the latter makes the dominant contribution. Substorms are, however, not triggered at the passage of the disturbances.

1. Introduction

[2] The magnetosphere is suddenly compressed at the time of passage of an interplanetary shock (IPS) [e.g., *Nishida*, 1978]. The sudden magnetospheric compression causes global and dynamic changes in the magnetic and electric fields and plasma motion in the magnetosphere and in the ionosphere. Sudden changes in the geomagnetic field are well known as a sudden commencement (SC) or a sudden impulse (SI) depending on whether or not a magnetic storm follows. SCs and SIs have been examined in a large number of studies [e.g., *Smith et al.*, 1986; *Araki*, 1994, and references therein] and result from the arrival of a compressional wave launched by an inward motion of the dayside magnetopause and propagating antisunward in the magnetosphere [e.g., *Wilson and Sugiura*, 1961; *Stegelmann and von Kenschitzky*, 1964; *Tamao*, 1964].

[3] Propagation of the compressional wave in the inner magnetosphere was studied by *Wilken et al.* [1982], who used multipoint observations of a SI by five spacecraft in the inner magnetosphere (around the geosynchronous orbit on the duskside) and one spacecraft in interplanetary space on the duskside. On the basis of the time lags among the spacecraft, they calculated a mean velocity along the raypath connecting GEOS at 1300 LT with GOES at 1930 LT to be 910 ± 140 km/s. The raypath was nearly parallel to the shock normal estimated by *King et al.* [1982]. *Baumjohann et al.* [1983] examined plasma drift and magnetic field variations associated with a SI measured in the inner magnetosphere at L = 6.6 R_E near 0700 LT. The plasma drift was tailward at the time of the first SI signatures and then was rotated about 45 toward dusk during a velocity increase.

[1]Space Research Institute, Austrian Academy of Sciences, Graz, Austria.
[2]Institute of Geophysics and Planetary Physics, University of California, Los Angeles, California, USA.
[3]Institute of Space and Astronautical Science, Japan Aerospace Exploration Agency, Sagamihara, Japan.
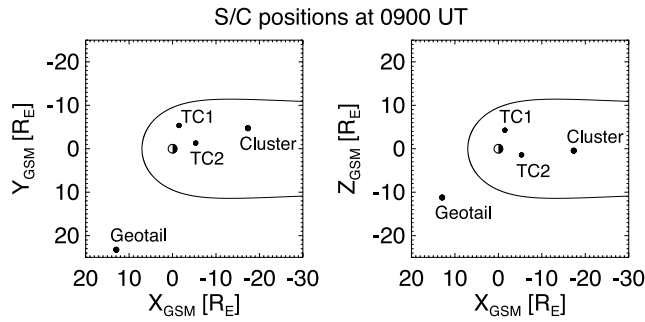[4]Max Planck Institute for Extraterrestrial Physics, Garching, Germany.
[5]Imperial College, London, UK.
[6]Centre d'Etude Spatiale des Rayonnements, CNRS/UPS, Toulouse, France.
[7]Institutet för Rymdfysik, Swedish Institute of Space Physics, Uppsala, Sweden.
[8]Space Science Laboratory, University of California, Berkeley, California, USA.

Figure 1. Positions of Geotail, DSP/TC1 and TC2, and Cluster at 0900 UT on 24 August 2005 in the (left) $X-Y$ plane and (right) $X-Z$ plane in GSM coordinates. The magnetopause is drawn with a thick curve, based on a model by *Shue et al.* [1998] with IMF B_z of 25.7 nT and solar wind dynamic pressure of 25.7 nPa as inputs.

[4] SIs in the magnetotail (tail SIs) have been also observed [*Patel*, 1968; *Sugiura et al.*, 1968; *Kawano et al.*, 1992; *Collier et al.*, 1998; *Kim et al.*, 2004; *Huttunen et al.*, 2005]. It has been suggested that tail SIs are mainly due to the lateral magnetotail compression caused by a magnetosheath pressure increase, rather than a compressional wave excited at the dayside magnetopause and propagating tailward as suggested by *Sugiura et al.* [1968]. *Kawano et al.* [1992] statistically examined the rotations of the magnetic field vectors during tail SIs and suggested that the lateral pressure effect on the tail boundary is the dominant cause of the rotation. *Kim et al.* [2004] examined a tail SI observed near the dusk magnetopause and estimated the propagation speed of the disturbance in the $X_{GSM}-R$ plane ($R = (X_{GSM}^2 + Y_{GSM}^2)^{1/2}$) with the use of three Cluster spacecraft. They estimated the propagation speed to be $\sim$320–380 km/s, which is comparable to the expected speed of the high-pressure solar wind in the magnetosheath. A detailed statistical study on magnetotail lobe compression was conducted by *Huttunen et al.* [2005], who applied the model developed by *Collier et al.* [1998] to fit Cluster observations. They estimated the disturbance propagation speed, which varied between $\sim$300 km/s and 900 km/s and was clearly of the order of the solar wind speed rather than of the order of the Alfvén speed ($>$1000 km/s) in the lobe. They suggested that the dominant cause of the lobe SIs is the lateral solar wind pressure enhancement.

[5] In spite of different studies mentioned above, there have been no studies that examined shock-associated disturbances in the plasma sheet with in situ observations. This is possibly because shock-associated disturbances are frequently contaminated by disturbances associated with a substorm. Although the shock-triggered substorms have been examined by a large number of studies [e.g., *Kokubun et al.*, 1977; *Zhou and Tsurutani*, 2001; *Liou et al.*, 2003; *Lyons et al.*, 2005; *Hubert et al.*, 2006], it is controversial whether or not magnetospheric compression itself has the potential to trigger a substorm. One of the key factors in this issue is how disturbances generated by magnetopause inward motion are propagating through the plasma sheet. In order to understand the propagation, it is necessary to examine the plasma sheet response with multipoint observations widely distributed in the magnetosphere.

[6] We examine a magnetospheric compression event which occurred near 0900 UT on 24 August 2005. We use data obtained by spacecraft distributed over different plasma regions: Geotail in the solar wind, Double Star Program (DSP) Tan Ce 1 (TC1) and Tan Ce 2 (TC2) in the inner magnetosphere, and Cluster in the plasma sheet. The simultaneous observations of compression-related disturbances enable us to compare the plasma sheet response with the response in the inner magnetosphere. In addition, we examine time lags of the disturbances among spacecraft to discuss global deformation of the compressional waves launched at the magnetopause. The data set used in the present study is introduced in section 2. In section 3, we show solar wind observations by Geotail, determine the shock normal, and show that the magnetosphere is globally compressed for the interval. In section 4 we show observations by DSP/TC1 and TC2 spacecraft. In section 5, we present Cluster observations and determine normal and speed of the front of disturbances. The results are summarized and discussed in section 6. In section 7 conclusions are drawn.

2. Data Set

[7] Figure 1 shows the locations of the spacecraft used in the present study. The Cluster spacecraft was located in the dawnside plasma sheet ($X_{GSM} = -17.4$ R$_E$, $Y_{GSM} = -4.7$ R$_E$, $Z_{GSM} = -0.48$ R$_E$). Magnetic field measurements are made by the Fluxgate Magnetometer (FGM) instrument [*Balogh et al.*, 2001]. FGM samples the magnetic field at about 202 vectors/s, and the highest-resolution data in the normal mode is at approximately 22 vectors/s. We use the 22 Hz data as well as 1-s data. The electric field is measured by the Electric Field and Wave (EFW) experiment [*Gustafsson et al.*, 1997, 2001]; we use spin-averaged 4-s data. Plasma data is provided by the Composition and Distribution Function (CODIF) analyzer of the Cluster Ion Spectrometry (CIS) experiment [*Rème et al.*, 2001], which can detect ions with energies from 40 eV/e to 40 keV/e and determine mass-per-charge of the incident ions. The energy is logarithmically divided into 14 ranges and angular coverage is $\sim$4π sr covered in 88 sectors for H$^+$ and O$^+$. Ion moment data such as density and velocity are calculated from the CODIF observations. We use 8-s data for both H$^+$ and O$^+$.

[8] We use magnetic field data obtained by the Magnetic Field Investigation (FGM) instrument on board DSP/TC1 [*Carr et al.*, 2005]. The data are averaged over a spin, which is around 4 s. We also use 1-s magnetic field data obtained by FGM onboard DSP/TC2 [*Carr et al.*, 2005]. TC1 is located at ($X_{GSM} = -1.5$ R$_E$, $Y_{GSM} = -5.3$ R$_E$, $Z_{GSM} = 4.2$ R$_E$) and TC2 is at ($X_{GSM} = -5.2$ R$_E$, $Y_{GSM} = -1.2$ R$_E$, $Z_{GSM} = -1.8$ R$_E$) for the interval of interest. The Hot Ion Analyzer (HIA) instrument on board TC1 provides 5 eV/e to 32 keV/e ion data with no mass determination [*Rème et al.*, 2005].

[9] We use solar wind and interplanetary magnetic field data obtained by the Solar Wind Analyzer (SWA) of the Comprehensive Plasma Instrumentation (CPI) [*Frank et al.*, 1994] and the magnetic field measurements (MGF) system [*Kokubun et al.*, 1994] onboard the Geotail spacecraft located at ($X_{GSM} = 13.0$ R$_E$, $Y_{GSM} = 23.2$ R$_E$, $Z_{GSM} = $
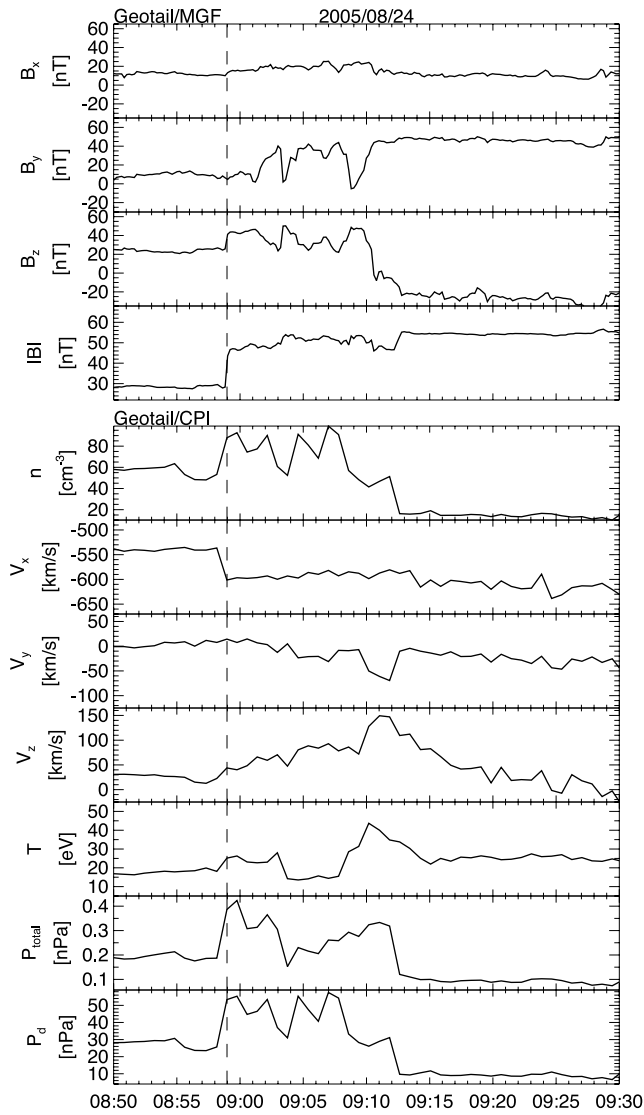
Figure 2. (top) IMF observed by Geotail/MGF. (bottom) Ion density, the *X*, *Y*, and *Z* components of ion velocity, ion temperature, the total pressure, and dynamic pressure of the solar wind observed by Geotail/CPI. The arrival of an interplanetary shock is indicated by dashed lines.

-11.2 R$_E$). Time resolution is 48 s for CPI data and 3 s for MGF data.

[10] Auroral images used in this study are obtained by the Far Ultraviolet imager (FUV) on board the Imager for the Magnetopause-to-Aurora Global Exploration (IMAGE) spacecraft, which is located at (X_{GSM} = 0.11 R$_E$, Y_{GSM} = 0.39 R$_E$, Z_{GSM} = -7.1 R$_E$) and observes the aurora every 2 min spin period [*Mende et al.*, 2000a]. The Wideband Imaging Camera (WIC) of FUV [*Mende et al.*, 2000b] measures emissions from the N$_2$ LBH-band and atomic NI lines.

[11] As a measure of low-latitude geomagnetic variations, we use the *SYM-H* index, which is essentially the same as the *Dst* index except that it is derived from six midlatitude stations and its time resolution is 1 min [*Iyemori*, 1990]. We

also use 1-s magnetic field data obtained at the Kakioka (KAK) observatory.

3. Magnetospheric Compression by an Interplanetary Shock

3.1. Shock Arrival

[12] An IPS arrived at Geotail upstream of the bow shock around 0859 UT. Figure 2 displays the interplanetary magnetic field (IMF) and ion density, ion velocity, ion temperature, the total pressure, and dynamic pressure of the solar wind observed by Geotail. The IPS is indicated by dashed vertical lines, characterized by sudden and simultaneous increases in the magnitude of IMF, ion density, ion velocity, ion temperature, and dynamic pressure.

[13] We estimate the normal direction of the IPS. We calculate the shock normal (**n**) with the use of the mixed data method [*Abraham-Shrauner and Yun*, 1976] which is based on the coplanarity theorem [*Colburn and Sonett*, 1966]:

$$\mathbf{n} = \pm \frac{(\mathbf{B}_1 - \mathbf{B}_2) \times [(\mathbf{B}_1 - \mathbf{B}_2) \times (\mathbf{V}_1 - \mathbf{V}_2)]}{|(\mathbf{B}_1 - \mathbf{B}_2) \times [(\mathbf{B}_1 - \mathbf{B}_2) \times (\mathbf{V}_1 - \mathbf{V}_2)]|},$$

where **B** and **V** are the magnetic field vector and plasma bulk velocity, and the subscripts 1 and 2 refer to the quantities ahead of and behind the shock, respectively. Given the shock normal (**n**), we can calculate the normal component of the shock velocity on the basis of mass flux conservation,

$$V_{shock} = \frac{(\rho_2 \mathbf{V}_2 - \rho_1 \mathbf{V}_1) \cdot \mathbf{n}}{\rho_2 - \rho_1},$$

where ρ_1 and ρ_2 is the upstream and downstream solar wind mass density, respectively. We used magnetic field data averaged over 1 min and the quantities ahead of and behind the shock indicated by the dashed lines in Figure 2. Solar wind data were averaged over two steps of data sampling in each quantity. The estimated normal direction and shock normal velocity are (ϕ, θ) = (175°, 13°), where ϕ and θ are the longitude and latitude in GSM coordinates, and V_{shock} = 692 km/s.

3.2. Entire Magnetospheric Compression

[14] Figure 3 presents the pressure profile of the sudden impulses observed in the magnetosphere and on the ground. From the top, the figure plots the solar wind dynamic pressure observed by Geotail, the *SYM-H* index, the geomagnetic *H* component measured at KAK, the total pressure at the position of TC1, magnetic pressure at the position of TC2, and the total pressure calculated from Cluster S/C 4 observations of the magnetic field and 40 eV to 40 keV H$^+$ and O$^+$ flux. The geomagnetic *H* component and the total pressure are parameters greatly affected by compression of the magnetosphere. The magnetic pressure profile can be used to monitor the magnetospheric compression when plasma β is low as in the inner magnetosphere. Although the plasma pressure at TC2 is unknown, it is reasonable to assume that the magnetic pressure dominates the total pressure at TC2 located at the radial distance of 5.6 R$_E$. The magnetic pressure shows in fact a similar time profile to
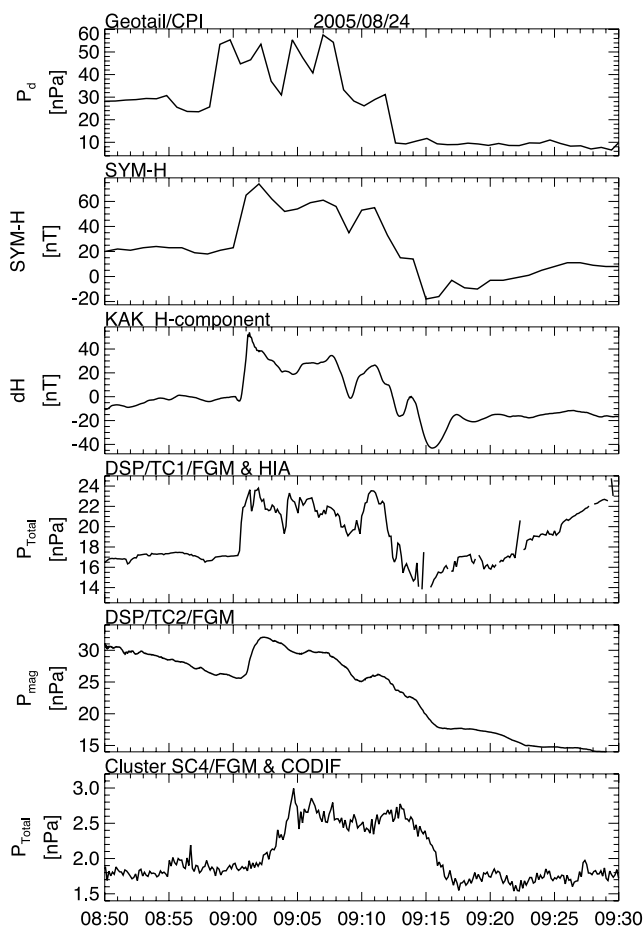
Figure 3. From the top, dynamic pressure of the solar wind observed by Geotail/CPI, the *SYM-H* index, the *H* component of the geomagnetic field at the Kakioka observatory, the total pressure at DSP/TC1, magnetic pressure at DSP/TC2, and the total pressure at Cluster S/C 4. All parameters show similar time profile: a sudden increase followed by a relatively gradual decrease down to a value smaller than the preincreased level.

the solar wind dynamic pressure: a sudden increase followed by a relatively gradual decrease down to a value smaller than the preincreased level. Note that a gradual decrease through the whole interval at TC2 is caused by spacecraft traveling toward the lower-magnetic field region. The similar profiles among the sudden impulses strongly suggest that an increase in the dynamic pressure of the solar wind caused the entire magnetospheric compression between ∼0900 and ∼0915 UT.

3.3. Auroral Activity

[15] Figure 4 shows a sequence of auroral images obtained by IMAGE/FUV/WIC from 0858:25 UT to 0917:11 UT. Each image is presented in a magnetic local time (MLT)-magnetic latitude grid with local noon at the top, dawn to the right, midnight at the bottom, and dusk to the left. The first panel (0858:25 UT) indicates two localized auroral brightenings near midnight and around 0130 MLT before the arrival of the shock at the magnetosphere. At 0900:30 UT, when the shock started to compress the

magnetosphere, auroral brightening occurred around the poleward boundary on the dayside. At 0902:35 UT, oval auroral luminosity was suddenly intensified on the night side at a wide range of MLT (19–6 MLT). The aurora remained intense until 0913:01 UT without any signatures of expansion at any directions, being therefore different from a usual substorm auroral bulge. It reduced gradually from 0913:01 UT. The oval aurora was intensified for about 15 min, which is consistent with the duration of magnetospheric compression indicated by pressure profiles in Figure 3. These observations clearly indicate that the auroral intensification is associated with magnetospheric compression, in particular compression of the near-Earth magnetotail.

4. Double Star Observations in the Inner Magnetosphere

[16] The top two panels of Figure 5 show the magnetic field intensity measured by FGM and the *X*, *Y*, and *Z* components of ion velocity in GSM coordinates (V_x, V_y, and V_z) observed by HIA on board DSP/TC1. The magnetic field increased suddenly at 0900:30 UT. At the same time of the increase, fast tailward plasma flow of ∼200 km/s was observed. The flow speed decreased exponentially between 0900:40 UT and ∼0902:20 UT; this decrease is quite similar to that reported in a previous study on plasma drift associated with the SI on 17 October 1978 [*Baumjohann et al.*, 1983]. The flow is caused by an inward motion of the dayside magnetopause due to the increased solar wind pressure. The plasma variation was (ΔV_x, ΔV_y) = (−141, 65) km/s and the longitude of the direction was $\phi = 155°$, and ΔV_z is almost constant ($\theta \sim 0°$) although a small fluctuation is seen. It is reasonable to focus on a compression-related variation of physical parameters, not on the absolute value or vector, since we are investigating the plasma response to the magnetospheric compression, namely, changes of the magnetospheric configuration and associated plasma motion.

[17] The bottom panel of Figure 5 plots the magnetic field intensity observed by FGM onboard DSP/TC2. Magnetic field disturbances started on 0901:00 UT.

5. Cluster Observations in the Plasma Sheet
5.1. Magnetic Field Variations and Plasma Flow

[18] Figure 6 shows magnetic field and ion observations made by Cluster S/C 4 in the plasma sheet from 0900 UT to 0910 UT. The top panel includes variations of *X*, *Y*, and *Z* components of the magnetic field (B_x, B_y, and B_z) observed by FGM in GSM coordinates. B_x and B_y show considerable variations during the interval. B_x was lower than 5 nT before it suddenly increased on 0904:15 UT. It reached more than 30 nT about 30 s later. B_y started to decrease around 0903:00 UT and reaches ∼0 nT right before 0905:00 UT. B_z was large for the whole interval; it was ∼20 nT from 0902:00 UT to 0903:00 UT, started to increase on 0903:00 UT, and reached a peak of about 35 nT on 0904:20 UT.

[19] The second panel shows ion velocity observed by CIS/CODIF in GSM coordinates. Solid and dotted lines indicate proton and oxygen velocity components, respectively. Both species display similar variations. Tailward
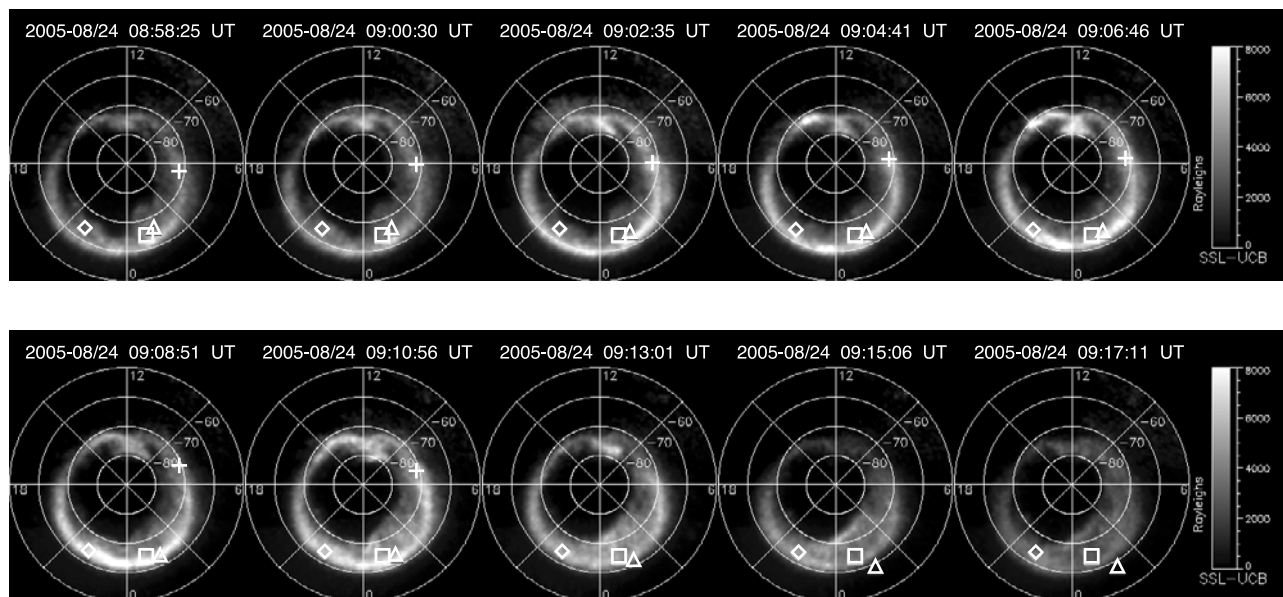
Figure 4. A sequence of aurora images obtained by IMAGE/FUV. Each image is presented in a MLT-magnetic latitude grid with 0 MLT at the bottom, 6 MLT to the right, 12 MLT at the top, and 18 MLT to the left. The triangle, plus, square, and diamond embedded in each image represent foot points of Cluster S/C 4, DSP/TC1 and TC2, and LANL/1994−084, respectively.

flow was observed at 0902:50 UT, followed by duskward and tailward flow (~230 km/s at maximum) around 0904:00–0904:40 UT.

[20] The third panel presents the X, Y, and Z components of the vector, $-V \times B$, in GSM coordinates, where V is the averaged ion velocity of H$^+$ and O$^+$ and B is the magnetic field. The X component started to decrease after 0903 UT, peaked at about -6 mV/m around 0904:30 UT, and increased up to 0 mV/m around 0905:30 UT. The Y component decreased to about -2 mV/m at 0902:50 UT and was negative in most of the interval until 0904:40 UT. The Z-component increased to about 2 mV/m at 0902:50 and further up to ~6 mV/m around 0904:30 UT. The bottom panel plots the X and Y components of the electric field in GSE coordinates. The black solid line is the electric field (E) observed by EFW in spacecraft coordinates which is almost the same as in GSE coordinates, and the dotted line is the corresponding component of $-V \times B$ in GSE coordinates. E is in good agreement with $-V \times B$. This fact and the agreement between the H$^+$ and O$^+$ velocities indicate that the plasma is convecting due to the enhanced E.

[21] All of the above-mentioned parameters experienced considerable and sudden changes between 0903 and 0904 UT, i.e., when the total pressure increased, as shown in the bottom panel of Figure 3.

5.2. Normal Direction and Propagation Speed of the Front

[22] Cluster S/C 4 observations in the plasma sheet between 0903 UT and 0905 UT showed considerable disturbances of the magnetic field and plasma motion (see section 5.1). Since the sudden changes are caused by magnetotail compression, the front of the disturbances is expected to be propagating from the magnetopause.

[23] In the present section, we examine the normal direction and propagation speed under the assumption of a planar front, utilizing the time lags of compression-related magnetic field disturbances between the four Cluster space-
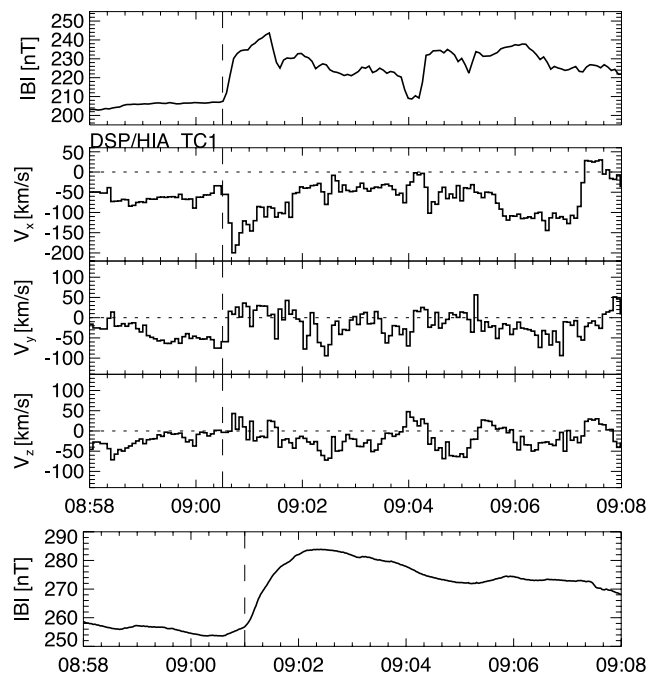
Figure 5. (top) Magnitude of the magnetic field and (middle) the X, Y, and Z components of ion velocity observed by DSP/TC1. The dashed lines indicate the onset of disturbances associated with magnetospheric compression. (bottom) Magnitude of the magnetic field observed by DSP/TC2. The onset of its change is indicated by the dashed line.
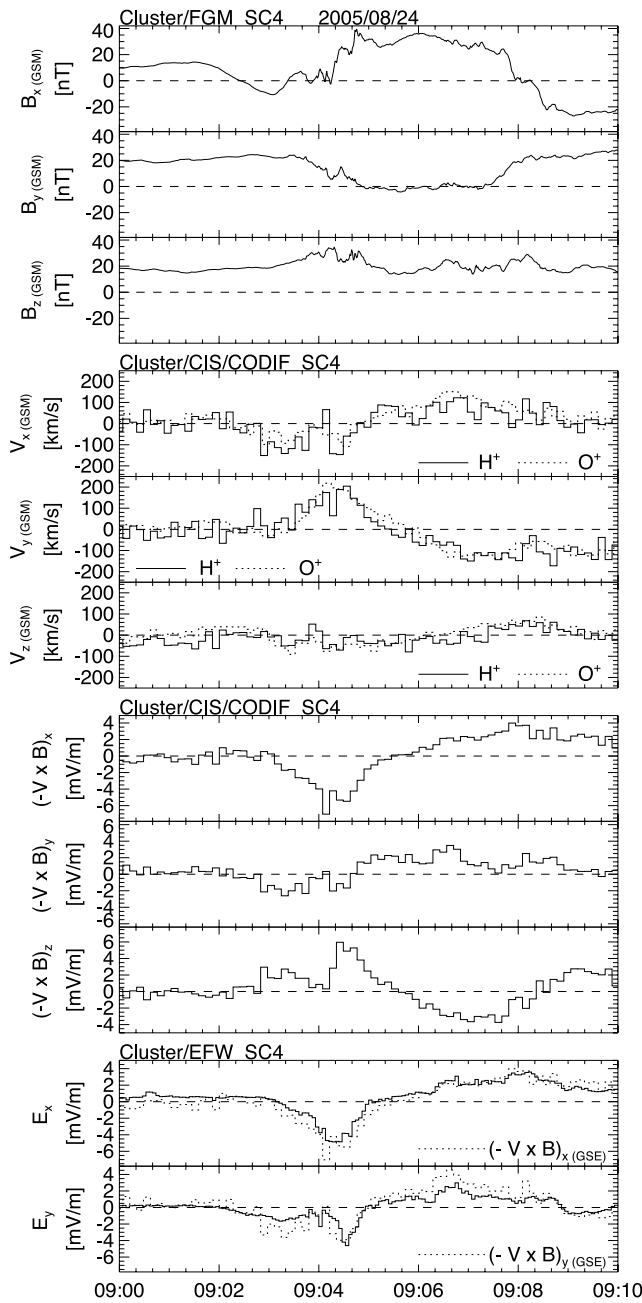
Figure 6. Observations by Cluster S/C 4. From the top is shown the magnetic field, velocities of H$^+$ (solid lines) and O$^+$ (dotted lines), three components of a vector, $-V \times B$ in GSM coordinates, and the electric field measured by EFW in spacecraft coordinates, overplotting the X and Y components of the $-V \times B$ vector in GSE coordinates.

craft. The spacecraft separation distances were smaller than 7000 km. With the help of the timing method [*Russell et al.*, 1983; *Harvey*, 1998], the normal and speed can be calculated on the basis of the following equation:

$$\begin{pmatrix} \Delta \mathbf{R}_{14} \\ \Delta \mathbf{R}_{24} \\ \Delta \mathbf{R}_{34} \end{pmatrix} \cdot \begin{pmatrix} N_x \\ N_y \\ N_z \end{pmatrix} = V \begin{pmatrix} \Delta t_{14} \\ \Delta t_{24} \\ \Delta t_{34} \end{pmatrix},$$

where $\Delta \mathbf{R}_{14}$, $\Delta \mathbf{R}_{24}$, and $\Delta \mathbf{R}_{34}$ and Δt_{14}, Δt_{24}, and Δt_{34} are the separations in space and time between spacecraft 4 and spacecraft 1, 2, and 3, respectively; V is the propagation speed; and N_x, N_y, and N_z are X, Y, and Z components of the normal vector, respectively. We use 22 Hz high-resolution magnetic field data obtained by the four Cluster spacecraft. The high-resolution data enable us to apply the timing analysis to the spacecraft configuration in which S/C 3 and S/C 4 is only ~1000 km separated.

[24] Figure 7 is an overview of the magnetic field variations observed by the four Cluster spacecraft between 0900 UT and 0910 UT. As shown in section 5.1, the magnetic field changed considerably from 0903 UT to 0905 UT. B_z shows a gradual increase from ~0903 UT and peaks around 0904:00–0904:40 UT. We choose the B_z increase as a proxy for the magnetotail compression. A B_z increase is one of the most suitable indices that indicate magnetospheric compression, in particular in a B_z-dominant condition, as is always in the dayside magnetosphere near the magnetic equator. In fact, B_z was much larger than B_x in the plasma sheet before the compression-related disturbances. The B_z increase coincides with an increase in the total pressure (see Figure 3) and compression-related variations in V_y and E_x (see Figure 6); the coincidence also suggests that the B_z increase is suitable for a proxy for compression for the examined event.

[25] Figure 8 shows a detail of the B_z increase with the use of the 22 Hz high-resolution magnetic field data for S/C 1, 2, 3, and 4 from the top. The gradual B_z increase is seen for each spacecraft and the B_z peak lies at different time among spacecraft as indicated by dashed lines. We use the peaks as a reference of the timing analysis method. Figure 9 is the results of the timing analysis along with relative positions of the Cluster spacecraft in the $X-Y$ and $X-Z$ planes. The solid black bar and arrow in each panel illustrate the estimated front plane and normal direction, respectively. The normal vector was estimated to be $(\phi, \theta) = (131°, -4°)$, and the propagation speed to be 338 km/s. An
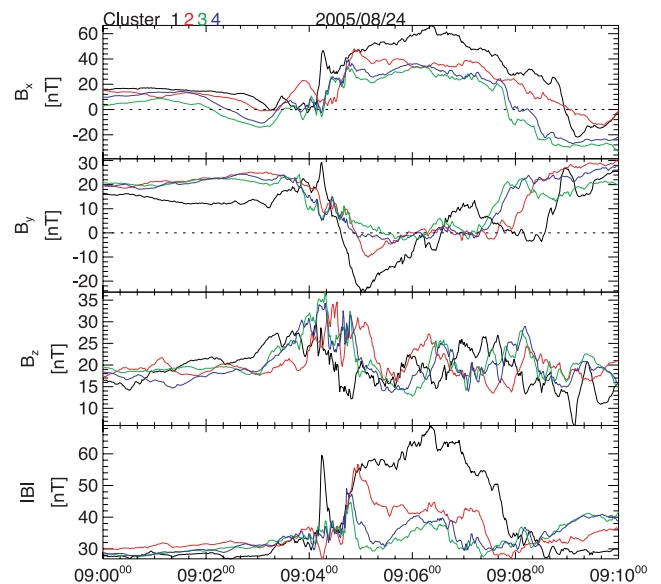
Figure 7. An overview plot of variations of the magnetic field observed by the four Cluster spacecraft.
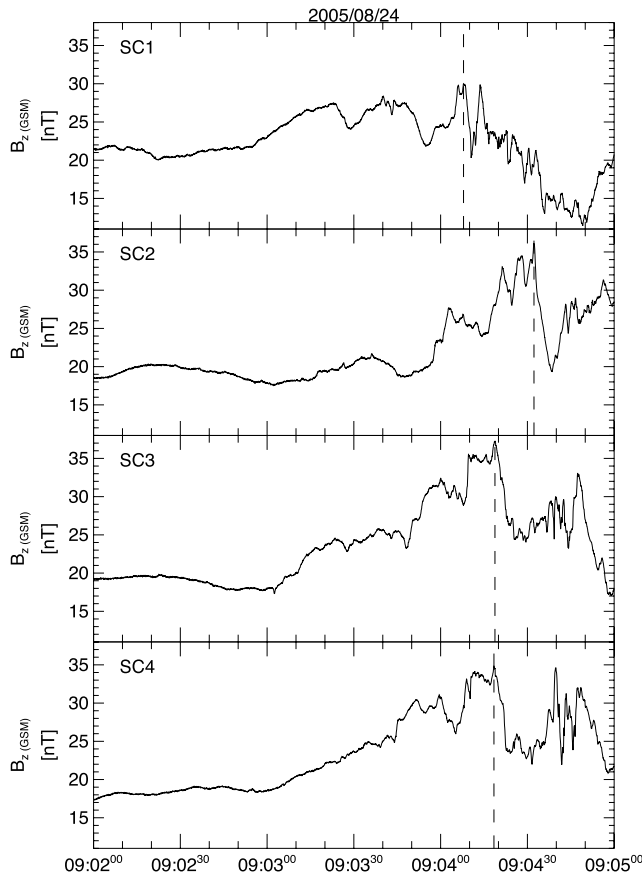
Figure 8. Variations of the Z component of the magnetic field observed by the four Cluster spacecraft. Dashed lines indicate peaks of the component, which we use as a reference of the timing analysis.

arrow denoted by E represents the direction of the $-V \times B$ vector calculated from Cluster S/C 4 observations around 0904:30 UT (see Figure 6). Since the X and Y components of the $-V \times B$ vector were almost the same as the measured electric field in GSE coordinates, we believe that the electric field can be expressed as $-V \times B$ during the present interval.

6. Summary and Discussion

[26] We investigated the response of the inner magnetosphere and the plasma sheet to a magnetospheric compression caused by an IPS around 0900 UT on 24 August 2005. The compression of the entire magnetosphere was confirmed by similar time profiles of the compression-related parameters in different plasma regions: the dynamic pressure of the solar wind at Geotail upstream of the bow shock, the *SYM-H* index, the geomagnetic H component measured at the Kakioka observatory, the total pressure at DSP/TC1 in the inner magnetosphere, the magnetic pressure at DSP/TC2 in the inner magnetosphere, and the total pressure at Cluster S/C 4 in the dawnside plasma sheet. Observed signatures at different locations are summarized in Table 1 and as follows:

[27] 1. The shock normal and speed was estimated to be $(\phi, \theta) = (175°, 13°)$, where ϕ and θ are the longitude and

latitude in GSM coordinates, and $V_{shock} = 692$ km/s, respectively, from solar wind observations by Geotail.

[28] 2. Fast plasma flow was observed by DSP/TC1 right after the onset of compression-related disturbances around 0900:30 UT. The plasma flow variation was $(\Delta V_x, \Delta V_y) = (-141$ km/s, 65 km/s$)$ $(\phi = 155°)$ and ΔV_z is almost constant $(\theta \sim 0°)$.

[29] 3. Magnetic field variations started around 0901:00 UT at DSP/TC2.

[30] 4. Disturbances of the magnetic and electric field and plasma flow were observed by Cluster S/C 4 after 0902:50 UT. The vector, $-V \times B$, where V is ion bulk velocity and B is the magnetic field, was in good agreement with the measured electric field.

[31] 5. The flow was tailward at 0902:50 UT. The longitude of the front normal of the disturbances was estimated to be $\sim 180°$ under the assumption that the electric field is on the front plane of compression-related disturbances and the normal of the front lies on the $X-Y$ plane.

[32] 6. The flow was duskward and slightly tailward around 0903–0905 UT. The front normal was estimated from the electric field and flow measurements to be $\phi = 107°$ at 0904:34 UT. The timing analysis, which utilized the time lags of arrival of the wavefront at the four Cluster spacecraft closely distributed one another also gave the normal and propagation speed of the front, which was estimated to be $(\phi, \theta) = (131°, -4°)$ and $V = 338$ km/s around 0904:20 UT.

[33] 7. Auroral brightening was suddenly intensified around $-60°$ to $-65°$ in magnetic latitude at a wide range of MLT from 0902:35 UT to 0913:01 UT. The intensification occurred during magnetotail compression but showed no typical signature of a substorm auroral bulge.

[34] Result 1 indicates that the IPS had the normal nearly parallel to the Sun-Earth line. We conclude that the shock compressed the magnetosphere nearly symmetrically with respect to the noon-midnight meridian. The conclusion can be also deduced from the risetime of the SIs, as discussed below.

[35] SI risetime is considered predominantly determined by the time required for the IPS front to sweep by the magnetosphere [*Nishida*, 1966; *Takeuchi et al.*, 2002; *Araki*
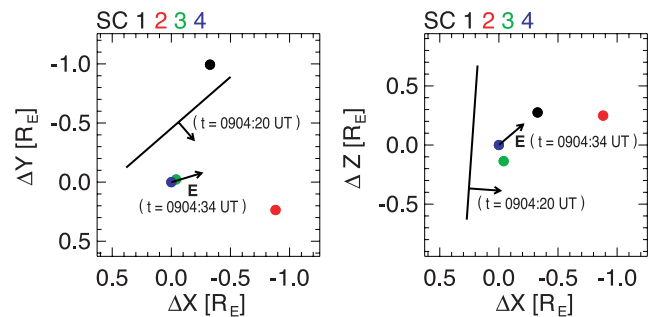
Figure 9. Separations of the four Cluster spacecraft and the results of the timing analysis in the (left) $X-Y$ and (right) $X-Z$ plane in GSM coordinates. Solid lines with arrows represent the estimated normal of the compression-related disturbances. Arrows denoted by **E** indicate the $-V \times B$ vector, which is almost consistent with the measured electric field.

Table 1. Summary of the Normal Direction of the Shock and the Compression-Related Disturbances

Spacecraft	Location	Time	X_{GSM}	Y_{GSM}	ϕ (longitude)	θ (latitude)
Geotail	solar wind (shock)	0858:49 UT	13.0 R$_{\mathrm{E}}$	23.2 R$_{\mathrm{E}}$	175°	13°
DSP/TC1	inner magnetosphere	0900:40 UT	−1.5 R$_{\mathrm{E}}$	−5.3 R$_{\mathrm{E}}$	155°	∼0°
DSP/TC2	inner magnetosphere	0901:00 UT	−5.2 R$_{\mathrm{E}}$	−1.2 R$_{\mathrm{E}}$	—	—
Cluster S/C 4 (Electric field and velocity observations)	plasma sheet	0904:34 UT	−17.4 R$_{\mathrm{E}}$	−4.7 R$_{\mathrm{E}}$	107°	0° (assuming)
Cluster S/C 1, 2, 3, and 4 (timing analysis)	plasma sheet	0904:08−32 UT	−17.4 R$_{\mathrm{E}}$	−4.7 R$_{\mathrm{E}}$	131°	−4°

et al., 2004], although there are several other candidates that may determine the risetime [Nishida, 1966]. Since the compression of the distant tail is not responsible for sudden impulses on the ground, there should be a "tailward edge" of the geoeffective magnetosphere; Takeuchi et al. [2002] defined the distance from the subsolar magnetopause to the tailward edge as "geoeffective magnetosphere length." The risetime becomes longer when the shock normal is inclined duskward or dawnward because the shock takes longer to sweep by the geoeffective magnetosphere length. The risetime of the SIs examined in the present study was shorter than 2 min in the inner magnetosphere as well as on the ground. In the following discussion of the shock inclination, we suppose that the shock passed the geoeffective magnetosphere length in 2 min. When the geoeffective magnetosphere length is assumed to be 30 R$_{\mathrm{E}}$, a shock with normal of $\phi = 120°$ must have the shock normal speed (V_{shock}) of ∼1960 km/s. Even a not-inclined shock with $\phi = 180°$ needs V_{shock} of ∼1600 km/s, which is much faster than our estimate from the local Geotail measurements. When we reduce the geoeffective magnetosphere length down to 15 R$_{\mathrm{E}}$, a shock with $\phi = 120°$ is still required to have a high V_{shock} (∼1550 km/s). A not-inclined shock ($\phi = 180°$), on the other hand, would have only to propagate with $V_{\mathrm{shock}} \approx 800$ km/s, comparable to our estimate from local measurements. We can therefore rule out the possibility that a highly inclined shock resulted in predominantly duskward propagation of the compression-related disturbances in the plasma sheet.

[36] In the following subsection, we discuss response of the inner magnetosphere and the plasma sheet to symmetric magnetospheric compression and deformation of the wavefront of compression-related disturbances.

6.1. Response to Magnetospheric Compression

[37] Figure 10a summarize the calculated shock normal and response of the inner magnetosphere and plasma sheet to magnetospheric compression in the $X−Y$ plane in GSM coordinates. The magnetopause is based on a model by Shue et al. [1998] with an upstream condition of the shock as input parameters; IMF B_{z} is 25.7 nT and solar wind dynamic pressure is 25.7 nPa. DSP/TC1 observed the flow variation on 0900:40 UT, which was mainly tailward and slightly duskward (result 2). As mentioned in section 4, an exponential decrease of the flow is quite similar to magnetospheric tailward and duskward plasma drift associated with the SI on 17 October 1978 [Baumjohann et al., 1983]. The plasma drift was well explained by an inward motion of the dayside magnetopause and propagation of the front of the magnetic field variations. We conclude that the flow variation observed at DSP/TC1 was caused by an inward motion of the dayside magnetopause due to the increased solar wind dynamic pressure. The front of the compression-

related disturbances is propagating predominantly tailward and slightly duskward. The propagation direction is indicated by an arrow at the position of TC1 in Figure 10a.

[38] Next, we estimate propagation speed in the inner magnetosphere, utilizing the time lag between Geotail and DSP/TC1 ($\Delta t = 111$ s) and the estimated shock speed ($V_{\mathrm{shock}} = 692$ km/s) and taking a raypath of propagation indicated by dotted lines in Figure 10a. The raypath is parallel to the shock normal outside of a model magnetopause and to the estimated propagation direction in the magnetosphere. We assume that a change in speed of the shock front in the magnetosheath is negligible [Spreiter and Stahara, 1994, Figure 5]. Numerical MHD modeling by Koval et al. [2005] and by Samsonov et al. [2006] demonstrated deceleration of the modeled IPS in the magnetosheath but by about only 10%. The propagation speed (V) is estimated to be ∼930 km/s. The time lag of onset times between DSP/TC1 (0900:30 UT) and DSP/TC2 (0901:00 UT) also allows us to estimate the propagation speed. Assuming that the normal of the wavefront is parallel to the shock normal, the propagation speed is calculated at 860 km/s. The estimated propagation speed (860−930 km/s) is comparable to propagation speed estimated from multispacecraft observations by Wilken et al. [1982] (770−1050 km/s) and by Andréeová and Pøech [2007] (714−741 km/s).

[39] Cluster S/C 4 observations indicate that compression-related disturbances were propagating down to the magnetotail. The front normal of the disturbances was estimated to be $\phi \sim 180°$ at 0902:50 UT (result 5). The dominant part of disturbances had the front normal of (ϕ, θ) = (131°, −4°) around 0904:20 UT and $\phi = 107°$ (assuming $\theta = 0°$) at 0904:34 UT (result 6), averaged at $\phi = 119°$. The averaged normal around 0904:30 UT is drawn with an arrow at the position of Cluster S/C 4 in Figure 10a. The flow and the disturbances are interpreted as a consequence of an inward (duskward) motion of the dawnside flank magnetopause due to an increase of the solar wind pressure in the magnetosheath. These features are not caused by the asymmetric compression that starts at a point dawnward of the subsolar point, as discussed above from the viewpoint of both shock normal and SI risetime. We conclude that lateral compression of the magnetotail made the dominant contribution to the compression-related disturbances in the plasma sheet. The plasma sheet response is similar to that of the magnetotail lobe [Kawano et al., 1992; Collier et al., 1998; Kim et al., 2004; Huttunen et al., 2005].

[40] Time lag among spacecraft can be utilized to estimate propagating speed of the wavefront in the plasma sheet, as it was for the estimate of the propagation speed in the inner magnetosphere. We take the time lag between Geotail and Cluster S/C 4 ($\Delta t = 328$ s) and a raypath

(a)

(b)
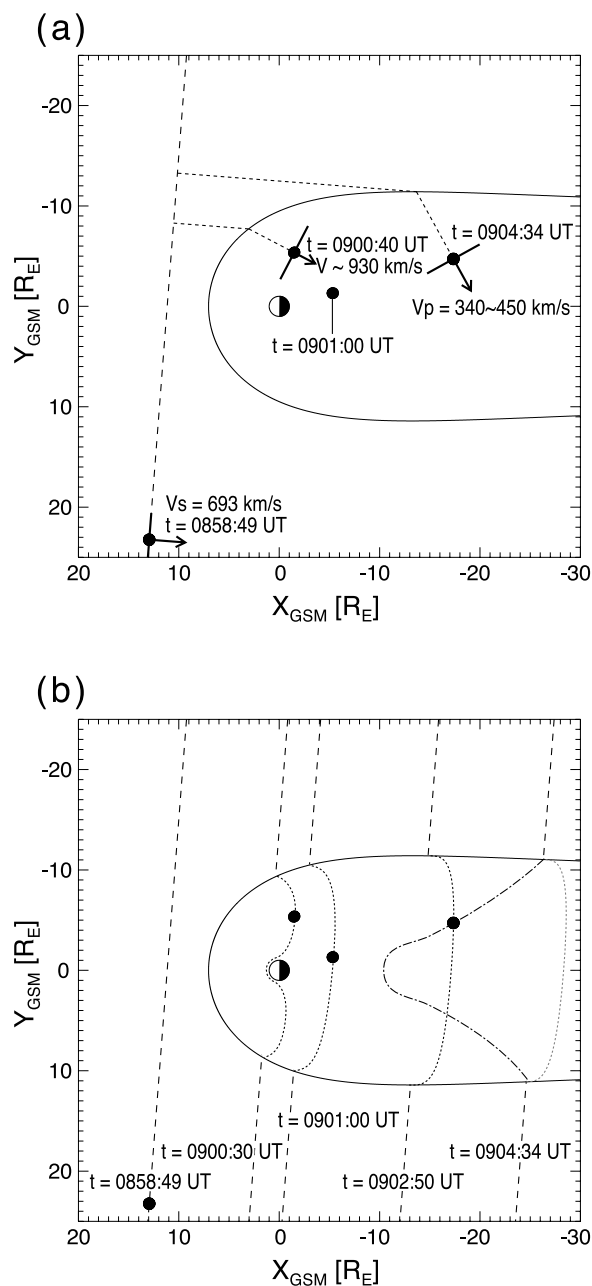
Figure 10. (a) Summary of the response of the inner magnetosphere and the plasma sheet to the magnetospheric compression due to an IPS. Solid small circles correspond to the positions of spacecraft shown in Figure 1. See text in section 6.1 in detail. (b) An illustration for propagation of the shock front and the compression-related disturbances of the magnetic field. Dashed, dotted, and dashed-dotted lines represent the shock front, the front of disturbances propagating from the dayside magnetopause, and the front propagating from the flank magnetopause, respectively. See text in section 6.2 in detail.

indicated by dotted lines in Figure 10a. The raypath is parallel to the shock normal outside of a model magnetopause and to the averaged propagation direction in the magnetosphere. The propagation speed in the plasma sheet

is estimated to be ~450 km/s, which is comparable to the speed estimated from the timing analysis (result 6).

6.2. Deformation of Compressional Waves

[41] Next, we discuss global deformation of compressional waves launched at the dayside and flank magnetopause. As addressed in section 6.1, we estimated propagation speed in the inner magnetosphere to be 860–930 km/s, using the time lags between Geotail, DSP/TC1, and DSP/TC2. The estimated speed is higher than the shock speed estimated at 692 km/s. Compressional waves launched at the dayside magnetopause were propagating in the magnetosphere faster than the shock sweeping by in the magnetosheath. Figure 10b illustrates propagation of the shock front (dashed lines) and the compressional waves (dotted lines). The front is drawn at 0900:30 UT and 0901:00 UT which are onset times at DSP/TC1 and DSP/TC2, respectively. Deformation of the compressional waves around the Earth takes into consideration a decrease in propagation speed in the plasmasphere. The decrease was not confirmed by in situ measurements in the present study but demonstrated by earlier studies [e.g., *Wilken et al.*, 1982].

[42] Since the compressional waves can propagate further down to the magnetotail, we estimate when the wavefront reaches the position of Cluster S/C 4. The arrival time was estimated to be 0902:30 UT under the assumption that propagation speed is 900 km/s. Cluster observations, on the other hand, showed increases in dawnward electric field and tailward plasma flow at 0902:50 UT (see Figure 6). We suggest that the increases were observed at the arrival of the compressional waves launched at the dayside magnetopause. The wavefront deformation at 0902:50 UT is indicated by a dotted line running through the position of Cluster S/C 4. The averaged propagation velocity from DSP/TC2 to Cluster S/C 4 is estimated to be 700 km/s when we utilize the time lag between the two spacecraft (i.e., 0901:00 UT at DSP/TC2 and 0902:50 UT at Cluster S/C 4). The speed is lower than that estimated in the inner magnetosphere. The difference could be explained by a probable reduction of speed of compressional waves because of a decrease in the Alfvén speed.

[43] Disturbances around 0904:30 UT, on the other hand, were propagating duskward from the dawnside magnetopause flank (see section 6.1). Since the shock front went further ahead at the time, waves from the dawnside magnetopause are deformed different from those launched at the dayside magnetopause. The deformation is drawn by a heavy dashed-dotted line running through the position of Cluster S/C 4. We speculate that the wavefront from the dayside magnetopause is propagating ahead of the shock front at 0904:30 UT, as illustrated by a light dotted line.

6.3. Triggering of Substorms

[44] Finally, we discuss the possible triggering of substorms at the time of passage of an IPS. For the event examined in the present study, Cluster in the dawnside plasma sheet observed an increase in B_z and duskward and tailward flow (~230 km/s at maximum) at 0904 UT. The B_z increase and flow are contrast to features frequently seen during dipolarization: B_z increases accompanied by earthward flow [e.g., *Baumjohann et al.*, 1991]. Auroral images obtained by IMAGE/FUV show sudden auroral

intensification at the time of magnetotail compression. The intensification occurred at a wide range of MLT almost simultaneously around auroral oval on the night side. The auroral brightening is consistent with previously reported global auroral intensification following the arrival of an IPS [*Chua et al.*, 2001; *Liou et al.*, 2003, *Lyons et al.*, 2005], being different from an auroral breakup and subsequent poleward expansion which are typically seen during substorm activity [e.g., *Untiedt et al.*, 1978]. There is no auroral bulge expanding azimuthally even in the global auroral enhancement. In addition to above mentioned observations, observations by LANL/1994−084 near 22 MLT and LANL/1990−095 near 6.5 MLT (not shown here) indicated no electron injection. We conclude that no substorm was triggered for the examined event, even though compression-related disturbances did pass through the plasma sheet tailward. The enhanced B_z disturbances in the plasma sheet, which resemble a signature of dipolarization, are not due to substorm activity but only magnetospheric compression. The nontriggering may be due to no considerable changes in IMF across the shock or/and prolonged strong northward IMF (shown in Figure 2), as proposed by earlier studies [*Liou et al.*, 2003; *Lyons et al.*, 2005].

7. Conclusions

[45] We investigated the response of the inner magnetosphere and the plasma sheet of the magnetospheric compression due to an increase in the solar wind dynamic pressure, utilizing observations of spacecraft distributed widely in different plasma regions: Geotail upstream of the bow shock, DSP/TC1 and TC2 in the inner magnetosphere, and Cluster in the dawnside plasma sheet. The magnetosphere was compressed symmetrically with respect to the noon-midnight meridian. The compression-related magnetic and electric field disturbances in the inner magnetosphere were due to magnetospheric compression at the dayside magnetopause. The dominant part of disturbances in the plasma sheet, on the other hand, were propagating from the flank magnetopause, although disturbances from the dayside magnetopause were also detected. We conclude that lateral compression of the magnetotail made the dominant contribution to the compression-related disturbances in the plasma sheet for the examined event. We showed that the plasma sheet disturbances can be explained by simple response to the sudden magnetospheric compression rather than internal processes such as substorm-associated disturbances.

References

Abraham-Shrauner, B., and S. H. Yun (1976), Interplanetary shocks seen by AMES plasma probe on Pioneer 6 and 7, *J. Geophys. Res.*, *81*, 2097−2102.

Andréeová, K., and L. Přech (2007), Propagation of interplanetary shocks into the Earth's magnetosphere, *Adv. Space Res.*, *40*, 1871−1880, doi:10.1016/j.asr.2007.04.079.

Araki, T. (1994), A physical model of the geomagnetic sudden commencement, in *Solar Wind Sources of Magnetospheric Ultra-Low-Frequency Waves*, *Geophys. Monogr. Ser.*, vol. 81, edited by M. J Engebretson, K. Takahashi, and M. Scholer, pp. 183−200, AGU, Washington, D.C.

Araki, T., T. Takeuchi, and Y. Araki (2004), Rise time of geomagnetic sudden commencements - Statistical analysis of ground geomagnetic data, *Earth Planets Space*, *56*, 289−293.

Balogh, A., et al. (2001), The Cluster magnetic field investigation: Overview of in-flight performance and initial results, *Ann. Geophys.*, *19*, 1207−1217.

Baumjohann, W., O. H. Bauer, G. Haerendel, and H. Junginger (1983), Magnetospheric plasma drifts during a sudden impulse, *J. Geophys. Res.*, *88*, 9287−9289, doi:10.1029/JA088iA11p09287.

Baumjohann, W., G. Paschmann, T. Nagai, and H. Lühr (1991), Superposed epoch analysis of the substorm plasma sheet, *J. Geophys. Res.*, *96*, 11,605−11,608, doi:10.1029/91JA00775.

Carr, C., et al. (2005), The Double Star magnetic field investigation: Instrument design, performance and highlights of the first year's observations, *Ann. Geophys.*, *23*, 2713−2732.

Chua, D., G. Parks, M. Brittnacher, W. Peria, G. Germany, J. Spann, and C. Carlson (2001), Energy characteristics of auroral electron precipitation: A comparison of substorms and pressure pulse related auroral activity, *J. Geophys. Res.*, *106*, 5945−5956, doi:10.1029/2000JA003027.

Colburn, D. S., and C. P. Sonett (1966), Discontinuities in the solar wind, *Space Sci. Rev.*, *5*, 439−506, doi:10.1007/BF00240575.

Collier, M. R., J. A. Slavin, R. P. Lepping, K. Ogilvie, A. Szabo, H. Laakso, and S. Taguchi (1998), Multispacecraft observations of sudden impulses in the magnetotail caused by solar wind pressure discontinuities: Wind and IMP 8, *J. Geophys. Res.*, *103*, 17,293−17,305, doi:10.1029/97JA02870.

Frank, L. A., K. L. Ackerson, W. R. Paterson, J. A. Lee, M. R. English, and G. L. Pickett (1994), The Comprehensive Plasma Instrumentation (CPI) for the Geotail spacecraft, *J. Geomagn. Geoelectr.*, *46*, 23−37.

Gustafsson, G., et al. (1997), The electric field and wave experiment for the Cluster mission, *Space Sci. Rev.*, *79*, 137−156, doi:10.1023/A:1004975108657.

Gustafsson, G., et al. (2001), First results of electric field and density observations by Cluster EFW based on initial months of operation, *Ann. Geophys.*, *19*, 1219−1240.

Harvey, C. C. (1998), Spatial gradients and the volumetric tensor, in *Analysis Methods for Multi-Spacecraft Data*, edited by G. Paschmann and P. W. Daly, pp. 307−348, ESA Publ. Div., Noordwijk, Netherlands.

Hubert, B., M. Palmroth, T. V. Laitinen, P. Janhunen, S. E. Milan, A. Grocott, S. W. H. Cowley, T. Pulkkinen, and J. C. Gérard (2006), Compression of the Earth's magnetotail by interplanetary shocks directly drives transient magnetic flux closure, *Geophys. Res. Lett.*, *33*, L10105, doi:10.1029/2006GL026008.

Huttunen, K. E. J., J. Slavin, M. Collier, H. E. J. Koskinen, A. Szabo, E. Tanskanen, A. Balogh, E. Lucek, and H. R. Rème (2005), Cluster observations of sudden impulses in the magnetotail caused by interplanetary shocks and pressure increases, *Ann. Geophys.*, *23*, 609−624.

Iyemori, T. (1990), Storm-time magnetospheric currents inferred from midlatitude geomagnetic field variations, *J. Geomagn. Geoelectr.*, *42*, 1249−1265.

Kawano, H., T. Yamamoto, S. Kokubun, and R. P. Lepping (1992), Rotational polarities of sudden impulses in the magnetotail lobe, *J. Geophys. Res.*, *97*, 17,177−17,182, doi:10.1029/92JA01250.

Kim, K. H., C. A. Cattell, D. H. Lee, A. Balogh, E. Lucek, M. Andre, Y. Khotyaintsev, and H. Rème (2004), Cluster observations in the magnetotail during sudden and quasiperiodic solar wind variations, *J. Geophys. Res.*, *109*, A04219, doi:10.1029/2003JA010328.

King, J. H., R. P. Lepping, and J. D. Sullivan (1982), On the complex state of the interplanetary medium of July 28−29, 1977, *J. Geophys. Res.*, *87*, 5881−5887, doi:10.1029/JA087iA08p05881.

Kokubun, S., R. L. McPherron, and C. T. Russell (1977), Triggering of substorms by solar wind discontinuities, *J. Geophys. Res.*, *82*, 74−86, doi:10.1029/JA082i001p00074.

Kokubun, S., T. Yamamoto, M. H. Acuna, K. Hayashi, K. Shiokawa, and H. Kawano (1994), The Geotail magnetic-field experiment, *J. Geomagn. Geoelectr.*, *46*, 7−21.

Koval, A., J. Šafránková, Z. Němeček, L. Prech, A. A. Samsonov, and J. D. Richardson (2005), Deformation of interplanetary shock fronts in the magnetosheath, *Geophys. Res. Lett.*, *32*, L15101, doi:10.1029/2005GL023009.

Liou, K., P. T. Newell, C. I. Meng, C. C. Wu, and R. P. Lepping (2003), Investigation of external triggering of substorms with Polar Ultraviolet Imager observations, *J. Geophys. Res.*, *108*(A10), 1364, doi:10.1029/2003JA009984.

Lyons, L. R., D. Y. Lee, C. P. Wang, and S. B. Mende (2005), Global auroral responses to abrupt solar wind changes: Dynamic pressure, substorm, and null events, *J. Geophys. Res.*, *110*, A08208, doi:10.1029/2005JA011089.

Mende, S. B., et al. (2000a), Far ultraviolet imaging from the IMAGE spacecraft. 1. System design, *Space Sci. Rev.*, *91*, 243–270, doi:10.1023/A:1005271728567.

Mende, S. B., et al. (2000b), Far ultraviolet imaging from the IMAGE spacecraft. 2. Wideband FUV imaging, *Space Sci. Rev.*, *91*, 271–285, doi:10.1023/A:1005227915363.

Nishida, A. (1966), Interpretation of SSC rise time, *Rep. Ionos. Space Res. Jpn.*, *20*, 42–44.

Nishida, A. (1978), *Geomagnetic Diagnosis of the Magnetosphere*, Springer, New York.

Patel, V. L. (1968), Sudden impulses in the geomagnetotail, *J. Geophys. Res.*, *73*, 3407–3418, doi:10.1029/JA073i011p03407.

Rème, H., et al. (2001), First multispacecraft ion measurements in and near the earth's magnetosphere with the identical Cluster Ion Spectrometry (CIS) experiment, *Ann. Geophys.*, *19*, 1303–1354.

Rème, H., et al. (2005), The HIA instrument on board the Tan Ce 1 Double Star near-equatorial spacecraft and its first results, *Ann. Geophys.*, *23*, 2757–2774.

Russell, C. T., M. M. Mellott, E. J. Smith, and J. H. King (1983), Multiple spacecraft observations of interplanetary shocks: Four spacecraft determination of shock normals, *J. Geophys. Res.*, *88*, 4739–4748, doi:10.1029/JA088iA06p04739.

Samsonov, A. A., Z. Němeček, and J. Šafránková (2006), Numerical MHD modeling of propagation of interplanetary shock through the magnetosheath, *J. Geophys. Res.*, *111*, A08210, doi:10.1029/2005JA011537.

Shue, J. H., et al. (1998), Magnetopause location under extreme solar wind conditions, *J. Geophys. Res.*, *103*, 17,691–17,700, doi:10.1029/98JA01103.

Smith, E. J., J. A. Slavin, R. D. Zwickl, and S. J. Bame (1986), Shocks and storm sudden commencements, in *Solar Wind-Magnetosphere Coupling*, edited by Y. Kamide and J. A. Slavin, pp. 345–365, Terra Sci., Tokyo.

Spreiter, J. R., and S. S. Stahara (1994), Gasdynamic and magnetohydrodynamic modeling of the magnetosheath - A tutorial, *Adv. Space Res.*, *14*, 5–19, doi:10.1016/0273-1177(94)90042-6.

Stegelmann, E. J., and C. H. von Kenschitzki (1964), On the interpretation of the sudden commencement of geomagnetic storms, *J. Geophys. Res.*, *69*, 139–155, doi:10.1029/JZ069i001p00139.

Sugiura, M., T. L. Skillman, B. G. Ledley, and J. P. Heppner (1968), Propagation of the sudden commencement of July 8, 1966, to the magnetotail, *J. Geophys. Res.*, *73*, 6699–6709, doi:10.1029/JA073i021p06699.

Takeuchi, T., C. T. Russell, and T. Araki (2002), Effect of the orientation of interplanetary shock on the geomagnetic sudden commencement, *J. Geophys. Res.*, *107*(A12), 1423, doi:10.1029/2002JA009597.

Tamao, T. (1964), A hydromagnetic interpretation of geomagnetic SSC*, *Rep. Ionos. Space Res. Jpn.*, *18*, 16–31.

Untiedt, J., R. Pellinen, F. Küppers, H. J. Opgenoorth, W. D. Pelster, W. Baumjohann, H. Ranta, J. Kangas, P. Czechowsky, and W. J. Heikkila (1978), Observations of the initial development of an auroral and magnetic substorm, *J. Geophys. Res.*, *45*, 41–64.

Wilken, B., C. K. Goertz, D. N. Baker, P. R. Higbie, and T. A. Fritz (1982), The SSC on July 29, 1977 and its propagation within the magnetosphere, *J. Geophys. Res.*, *87*, 5901–5910, doi:10.1029/JA087iA08p05901.

Wilson, C. R., and M. Sugiura (1961), Hydromagnetic interpretation of sudden commencements of magnetic storms, *J. Geophys. Res.*, *66*, 4097–4111, doi:10.1029/JZ066i012p04097.

Zhou, X. Y., and B. T. Tsurutani (2001), Interplanetary shock triggering of nightside geomagnetic activity: Substorms, pseudobreakups, and quiescent events, *J. Geophys. Res.*, *106*, 18,957–18,967, doi:10.1029/2000JA003028.

————————————

M. André, Institutet för Rymdfysik, Swedish Institute of Space Physics, Regementsv. 1, SE-752 37 Uppsala, Sweden.

W. Baumjohann, K. Keika, R. Nakamura, and T. L. Zhang, Space Research Institute, Austrian Academy of Sciences, Schmiedlstrasse 6, A-8042 Graz, Austria.

C. Carr and E. A. Lucek, Imperial College, Prince Consort Road, London SW7 2BZ, UK.

I. Dandouras and H. Rème, Centre d'Etude Spatiale des Rayonnements, CNRS/UPS, 9 Avenue du Colonel Roche, F-31028 Toulouse CEDEX 4, France.

H. Frey, Space Science Laboratory, University of California, Berkeley, 7 Gauss Way 7450, Berkeley, CA 94720-7450, USA.

B. Klecker and M. Volwerk, Max Planck Institute for extraterrestrial Physics, Karl-Schwarzschild-Straße 1, D-85741 Garching, Germany.

A. Runov, Institute of Geophysics and Planetary Physics, University of California, Box 951567, Los Angeles, CA 90095, USA.

T. Takada, Institute of Space and Astronautical Science, Japan Aerospace Exploration Agency, Yoshinodai 3-1-1, Sagamihara 229-8510, Japan.